Catalyst evaluation for high-purity H_2 production by sorption-enhanced steam-methane reforming coupled to a Ca/Cu process

M.V. Navarro*, J.M. López, T. García, G. Grasa, R. Murillo

Department of Energy and Environment, Instituto de Carboquímica (ICB-CSIC),

C/ Miguel Luesma Castán 4, 50018 Zaragoza, Spain

ABSTRACT

The operational limits of a commercial nickel-based catalyst under the conditions of a sorption-enhanced steam-methane reforming process coupled to a Ca/Cu chemical loop are investigated for high-purity H_2 production in a cyclic operation. The performance of the reforming catalyst is tested by means of a high number of oxidation-reduction-reforming cycles. After 100 oxidation-reduction cycles, this catalyst retains its exceptional reforming activity. The methane conversion values are close to the thermodynamic equilibrium under very demanding conditions: temperature between 500 ºC - 700 ºC and mass hourly space velocity of 8.8 $kgCH_4\ h^{-1}\ kgcat^{-1}$. After 200 cycles, the sample shows reduction in its reforming activity in line with a lower dispersion of the Ni species. Sintering of Ni nanocrystals is evidenced during the oxidation-reduction multi-cycles. The performance of the catalyst after 200 oxidation-reduction cycles mixed with a CaO-based CO_2 sorbent is studied under optimal conditions calculated for the sorption-enhanced reforming process coupled to a Ca/Cu cycle (temperature of 650 ºC, steam/methane ratio of 4, sorbent/catalyst ratio of 4 and space velocity of 0.75 $kgCH_4\ h^{-1}\ kgcat^{-1}$). Remarkably, an equilibrium value over 92

vol.% H_2 concentration is achieved, highlighting this catalyst as a promising candidate for the next steps of the process development.

Keywords: H_2 production, sorption-enhanced reforming, steam-methane reforming, combined calcium-copper cycle

Corresponding author. Tel: +34 976733977; fax: +34 976733318.

E-mail address: navarro@icb.csic.es (María Victoria Navarro)

1. Introduction

Hydrogen production worldwide is currently at a rate of more than 50 million tonnes per year [1], and its demand for both chemical and energy industries is expected to increase in the medium to long term [2]. Steam-methane reforming (SMR) is the most commonly used process for the production of hydrogen; however, this process emits high levels of CO_2, an average of close to 7 $kgCO_2$ kgH_2^{-1} [3], which is a by-product of the reforming process and the additional combustion of CH_4 required by the steam reformer. Therefore, SMR does not meet market requirements of low CO_2 emission levels and high-energy efficiency [4]. CO_2 capture is currently seen as a promising way to decrease global CO_2 emissions, and there is great interest worldwide in developing new CO_2 capture technologies for the purpose of reducing the energy penalty. The sorption-enhanced steam-methane reforming (SE-SMR) process for hydrogen production, may fulfil this need. The concept behind this process is based on the use of a reforming catalyst in combination with a selective regenerable solid sorbent to remove CO_2 in situ from the reaction zone [5]. This way, most of the 15–20% CO_2 present in the effluent gases from the SMR process can be captured. Additionally, CO_2 removal from the gas phase in the reaction zone shifts the equilibrium of the reversible reactions of SMR and water gas shift (WGS), enhancing hydrogen production from approximately 80% to 95% (dry basis) [6] based on Le Chatelier's principle. Other potential advantages of SE-SMR when compared to SMR have been already pointed out in the literature, such as the reduction in reaction temperature, lower by-product formation, elimination of WGS reactor, etc. [7], which is why this process has received much attention over the last two decades [8, 9]. However, the SE-SMR process requires the addition of a sorbent regeneration stage in order to be able to perform cyclically once the CO_2 sorbent is saturated. Accordingly, the SE-SMR process has been studied

in different configurations, such as fixed bed under atmospheric or high pressure, and in fluidized and bubbling bed systems [10]. Nevertheless, combined strategies for hydrogen production with CO_2 capture focused on reducing the associated costs and energy penalty are still at a very early stage of development.

J. C. Abanades et al. [11] have developed a process that uses the well-known principals of SE-SMR for H_2 production with $CaO/CaCO_3$ chemical loop, coupled to a second Cu/CuO chemical loop that solves the problem of endothermic $CaCO_3$ calcination [12]. There has been an intense work in the recent years for the further development of the Ca/Cu looping process for H_2 production and or power generation compiled in a recent overview by Fernandez and Abanades [13]. The initial works presented the conceptual design of the process [11,14] and relevant works have been focused on reactor modelling [7,15-17] and process integration [18-21] to demonstrate the implementation of the concept on large-scale H_2 production process. Reaction stages involving Ca and Cu solids have been experimentally studied at laboratory scale [22,23] and simultaneous CuO reduction/CaCO3 calcination up to TRL4 [24]. The experimental studies on SER stage under relevant conditions of the process are currently scarce nevertheless high H2 production efficiencies have been corroborated for a mixture of CO2-sorbent with fresh or aged reforming catalyst at different mass hourly space velocities and pressures [25]. The basic Ca/Cu looping process consists of a sequence of three main reaction steps (see Figure 1), which are adiabatically carried out in fixed-bed reactors operating in parallel at different reaction steps to make a continuous looping operation feasible. Narrow and precise operating windows have been defined for the conceptual design of the process [7,14,15]. Accordingly, the optimal operation conditions calculated for the reforming stage are 650 ºC–750 ºC, 5 bar–15 bar, a steam to carbon ratio of 3–6 and a mass flow velocity (CH_4+steam) of 3.5 kg m^{-2} s^{-1}. The high

exothermicity of Cu oxidation permits the generation of an exit gas stream at a high temperature of 830 ^{o}C to allow energy recovery [14] and the calcination reaction, together with the exothermic reduction of CuO, is carried out at a high temperature ranging between 850 ºC and 870 ºC. One of the actual challenges is to find appropriate materials that withstand the typical Ca/Cu process conditions and are able to work in multi-cyclic operation (oxidation-reduction/calcination-reforming cycles). A focus on the evolution of every material involved in the process in a high number of these multiple cycles is required before furthering the development of the technology.

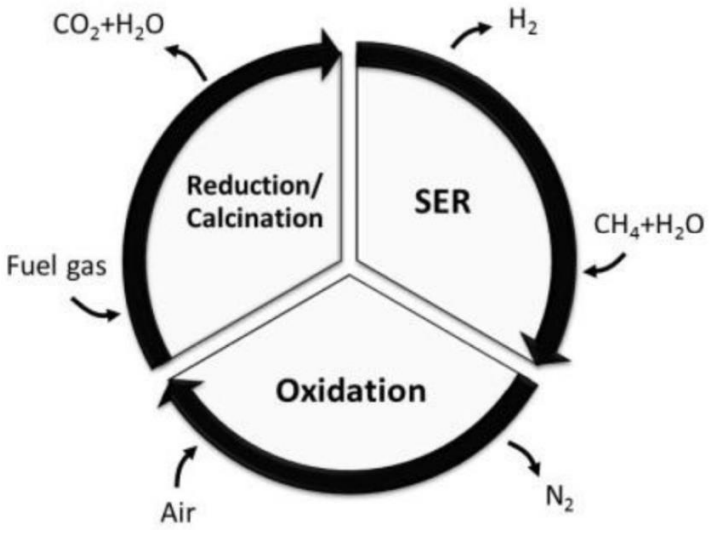

Fig. 1. H_2 production Ca/Cu looping process concept from Grasa et al. [25].

With regard to catalysts applicable to the SE-SMR process coupled to a Ca/Cu cycle, commercial SMR catalysts developed to be applied at high temperature and pressure (typically 800 ^{o}C–900 ^{o}C and 15 atm–20 atm) [3] have been used successfully in SE-SMR processes [26-40]. In these studies, the reforming step was carried out at remarkably reduced temperatures and pressures (400 ºC–750 ºC and 1 atm–15 atm) [26-40]. For the sorbent regeneration step, these studies changed temperature and reaction atmospheres to calcination conditions (550 ºC –1000 ºC, and steam, diluted air or inert

gas) [8,27,36-41]. Periodical changes in the catalyst environment produce enlargement and reduction of molar volumes from reduced metallic Ni^0 to oxidized NiO [10,36], which can negatively affect catalyst performance. Likewise, catalysts can suffer from carbon formation and oxidation by steam effect [42], formation of spinels [43], agglomeration of Ni crystallites [36], and Ni crystallite growth [37,42]. Although catalyst stability is a key parameter for the potential development of the process, there is little information regarding the effect of reforming-regeneration cycling on the activity of commercial catalysts for SMR [27,36-40]. In relation to the high number of cycles, Lysikov et al. [36] studied the influence of RedOx cycling in a pristine catalyst consisting of nano-sized nickel oxide with an average diameter of 5–10 nm and reported an increase in the active component of up to 100–200 nm after 100 cycles. Lopez-Ortiz and Harrison [37] reported a different increase in the Ni crystallites with regard to size and growth pattern depending on the regeneration temperature under an inert atmosphere. For the first 5 cycles the active phase presented a similar increase for both regeneration temperatures of 800 ºC and 950 ºC, to 25.4 nm and 26.3 nm, respectively. However, an additional increase occurred at 950 ºC with diameters reaching 32.2 nm in the 15^{th} cycle, compared to the increase in the crystallite produced by regeneration at 800 ºC, to 27.2 nm after 25 cycles.

The aim of the present research was to study the limits for application of a commercial catalyst provided by Johnson Matthey© (HiFUEL® R110) under conditions of SE-SMR coupled with a Ca/Cu chemical loop. The experiments were initially performed without sorbent to allow close monitoring of the reforming activity and the evolution of catalyst properties after multi-cyclic oxidation-reduction tests. To our knowledge, this is the first time in the literature that an evaluation has been made of catalyst performance during the cyclic operation of the SE-SMR process involving

reforming-oxidation-reduction stages. The material was placed in an atmospheric fixed bed reactor system and endured consecutive stages of oxidation at 850 ºC under O_2 rich atmosphere and reduction at 850 ºC with H_2, in an attempt to mimic the different stages defined in the process under study. Catalyst performance was evaluated under different conditions of temperature and mass hourly space velocity (MHSV). The catalyst was subsequently cycled through 200 oxidation-reduction steps in order to study its SMR catalytic stability and its performance in a proper SE-SMR process with a sorbent.

2. Experimental

A commercial SMR Ni-based catalyst with 15.9–20.0 wt% Ni content, as determined by element analysis within this current study, and supported on $CaAl_2O_4$ was supplied by Johnson Matthey, HiFUEL® R110. This solid was received in a 4-hole quadralobe pellet form, and was crushed and sieved to a particle size between 100 μm and 200 μm for the experiments.

A synthetic dolomite sorbent, CaO/MgO 2:1 molar ratio, was prepared using a co-precipitation method starting from the corresponding nitrate precursors provided by Scharlab S.L. A pH of 9 was used in the precipitation step, previous to a calcination step performed at 875 ºC in N_2 atmosphere for 2 h. The particle size range used in the experiments was 100 μm–200 μm. It presented 75 wt% CaO measured by ICP and evolution of its sorption capacity up to 100 carbonation-calcination cycles between 0.6 and 0.3 g CO_2 g^{-1} calcined sorbent.

SMR experiments were carried out with different amounts of catalyst ranging between 0.05 g and 0.20 g mixed with 0.62 g–2.5 g SiC provided by VWR Chemicals BDH Prolabo (201 μm average particle size). SiC was introduced to prevent dispersion problems and to reduce temperature changes. The sample was placed in a 300 mm

length tubular quartz reactor, with an inner diameter of 6.8 mm and a total bed length ranging between 10 mm and 40 mm. The reactor was located in a cylindrical, electrically heated oven controlled by a PID controller and a thermocouple positioned in the middle of the sample. The gas mixture was measured by a set of mass flow controllers calibrated for CH_4, H_2, O_2, Ar and water. The water flow was mixed with Ar and CH_4 and evaporated in a stainless-steel pipe heated to 400 ºC by a cylindrical electric furnace connected to a temperature controller. Ar was introduced at the same molar ratio as that of the water to favour the formation of small water droplets that would lead to a homogeneous steam flow and faster signal stabilization. The different feeding mixtures were stabilized in a secondary line before passing through the reactor where the catalyst was placed. A pressure gauge located before the reactor provided reaction pressure recording. A recovery system was positioned after the reactor to condense water. Finally, aliquots of the outlet gas stream were analysed online using a quadrupole spectrometer (Omnistar, Pfeiffer Vacuum) The following masses were monitored: m/z =2 for H_2, m/z =15 for CH_4, m/z=18 for water, m/z = 28 for CO, m/z=32 for O_2 m/z = 40 for Ar, and both m/z= 28 and 44 for CO_2.

The routine for the tests conducted at the experimental facility was as follows: before each reforming test, the catalyst was heated in Ar atmosphere and then reduced in situ for 30 min at 850 ºC with 10 vol.% H_2 balanced by Ar (total flow 33.3 mlN min^{-1}). The catalytic activity of the sample was subsequently measured at 500 ºC, 550 ºC, 600 ºC, 625 ºC, 650 ºC, 675 ºC and 700 ºC for 30 minutes each. A steam to methane ratio of 3 and MHSV of 2.0 $kgCH_4$ h^{-1} $kgcat^{-1}$ were used. Ten consecutive oxidation-reduction cycles were then performed in situ. The samples were first oxidized for 30 min at 850 ºC with 10 vol.% O_2 balanced by Ar (total flow 33.3 mlN min^{-1}), and then reduced under the previously mentioned reduction conditions. Finally, the reforming

activity of the catalyst was tested again after the tenth cycle at the same temperature plateaus. In addition, replicate tests were performed but at different MHSVs of 4.3 $kgCH_4\ h^{-1}\ kgcat^{-1}$ and 8.8 $kgCH_4\ h^{-1}\ kgcat^{-1}$. The mass balances to carbon species was closed in all runs above 85%.

A TGA apparatus was used to age the catalyst to an increasing number of oxidation-reduction cycles. Briefly, the TGA apparatus consisted of a quartz tube with a suspended platinum basket that was positioned inside a furnace. The temperature and sample weight were continuously recorded by computer. The reacting gas mixture was regulated by means of mass flow controllers and fed in through the bottom of the quartz tube. The routine for the TGA cycling consisted of: (1) heating up to 850 ºC in N_2; (2) a 5-minute reduction stage at 850 ºC with 10 vol.% H_2 balanced by N_2; (3) 1 minute in N_2 atmosphere; and (4) a 5-minute oxidizing stage with 20 vol.% O_2 balanced by N_2. The reduction-oxidation routine was repeated up to 200 times. About 70 mg of the sample was introduced in the platinum basket in the TGA. After cycling, the sample was cooled down to room temperature in N_2 atmosphere.

The main properties of the fresh catalyst and sorbent were analysed by different characterization techniques. Particle density was measured in a Micromeritics Accupyc II 1340 He pycnometer. Surface area was determined by the Brunauer-Emmet-Teller (BET) method by adsorption/desorption of Nitrogen at -196 ºC in a Micromeritics ASAP 2020. The mean pore size value was calculated by means of the BJH method from the adsorption branch. Hg porosimetry was used in a Quantachrome Poremaster to analyse sample porosity. Powder X-ray diffraction (XRD) spectroscopy was utilized to identify the crystalline phases present in the fresh and cycled samples, by means of a Bruker D8 Advance diffractometer with monochromatic Cu Kα source operated at 40 kV and 40 mA. The experimental patterns were calibrated against a silicon standard and

the crystalline phases were identified by matching the experimental patterns to the JCPDS powder diffraction file database. Scanning electron microscopy (SEM) and Transmission electron microscopy (TEM) were also applied to fresh and cycled samples in order to determine the evolution of the nickel distribution on the support with the cyclic operation. A Hitachi S-3400 N model coupled to a Röntec XFlash EDX and a JEOL-2000FXII microscope coupled to an INCA 200-X SIGHT analyser were used, respectively. The fresh catalyst was characterized by sequential temperature programmed reduction/temperature programmed oxidation (TPR/TPO) analysis. A total of ten cycles were carried out, allowing the evolution of catalyst reducibility with cyclic operation to be followed. This information can be used to estimate the content and nature of the reducible species present in the fresh catalyst and their evolution throughout the oxidation-reduction cycles. The analysis was performed in a PulseChemisorb 700 of Micromeritics with an initial stabilization step of 30 minutes at 150 ºC in Ar atmosphere (30 mlN min^{-1}), followed by a cooling step up to 45 ºC. At this temperature, the sample was stabilized for 15 min in 10 vol.% H_2 balanced by Ar (30 mlN min^{-1}) before the temperature was increased at a heating rate of 10 ºC min^{-1} up to 850 ºC. Finally, this temperature was held for 30 minutes. After a cooling step in Ar, TPO was carried out under the same conditions as those of the reduction stage but with an oxidizing atmosphere of 10 vol.% O_2 in Ar.

3. Results and discussion

3.1. Physicochemical properties of fresh materials

The textural characterization of the fresh materials is summarised in Table 1. Values are in the range of data previously presented in the literature [44-46].

Table 1
Main textural properties of the fresh materials.

	Density, g cm^{-3}	Porosity	SBET, m^2 g^{-1}	Mean pore size, nm
HiFUEL R110	3.4	0.41	25	14
CaO/MgO 2:1	2.6	0.54	16	80

Figure 2 shows the XRD patterns of the catalyst after an increasing number of oxidation-reduction-reforming cycles. The XRD pattern of the initially reduced catalyst at the bottom of the figure shows that the only Ni-based crystallite phase present is metallic Ni. The characteristic peaks of Al_2O_3, $CaO(Al_2O_3)_2$ and $CaO(Al_2O_3)$ phases corresponding to the support can also be observed. From this pattern, the initial Ni crystallite size is calculated by the Rietveld method to be 9 nm.

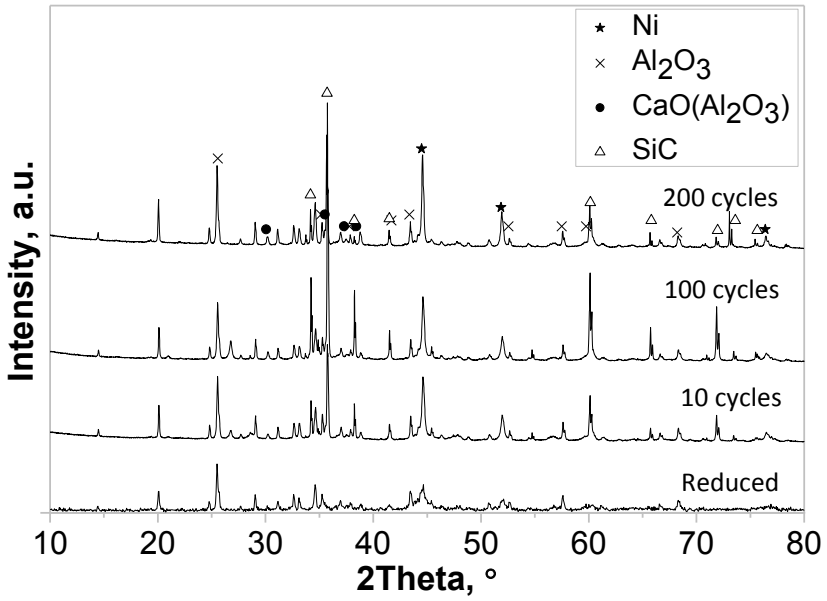

Fig. 2. XRD patterns of reduced Ni catalyst after an increasing number of oxidation-reduction cycles. Unattributed peaks correspond to the $CaO(Al_2O_3)_2$ phase present in the support.

Some catalyst particles were analysed by SEM-EDX after an increasing number of oxidation-reduction-reforming cycles to determine possible morphological changes produced during cycling. The SEM image of the initially reduced catalyst in Figure 3.a shows a homogeneous Ni distribution over the support surface with only few visible small white spots (identified by EDX) with small grain size.

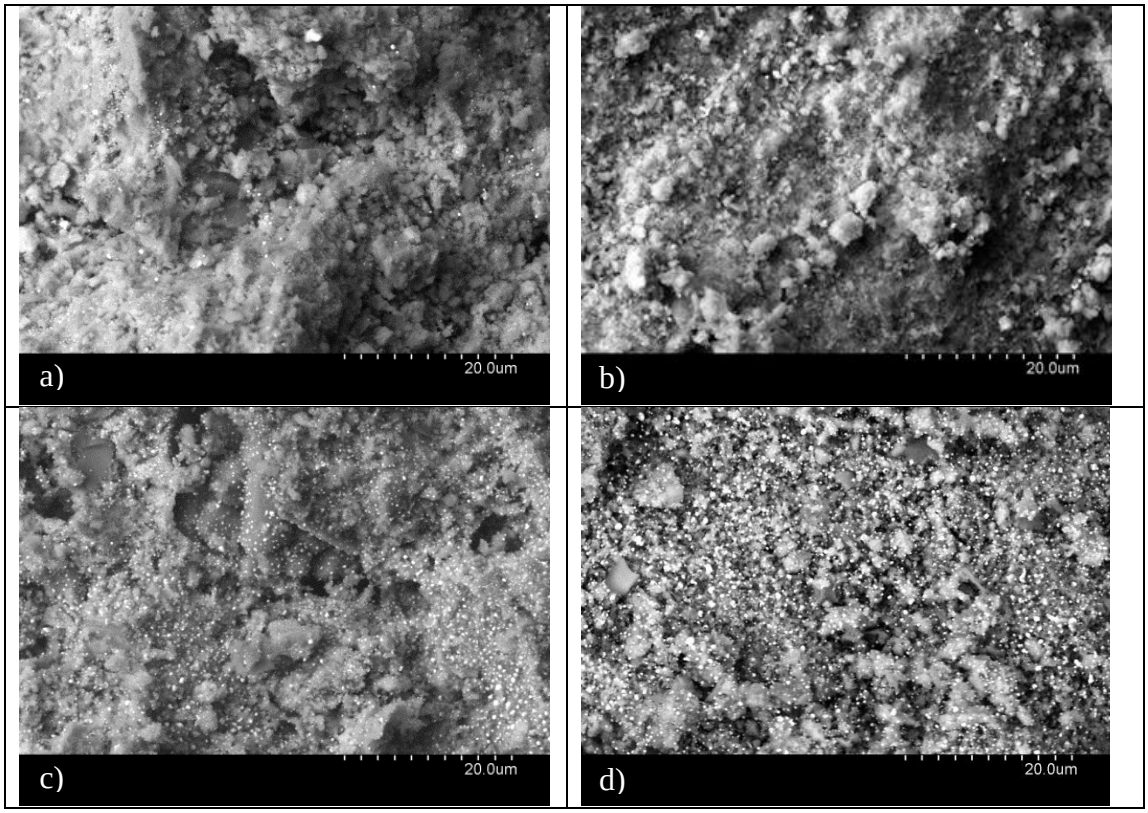

Fig. 3. SEM images of reduced Ni catalyst after an increasing number of oxidation-reduction cycles. a) reduced, b) 10 cycles and used, c) 100 cycles and used, d) 200 cycles and used.

Examination of the reduced catalyst by TEM (Figures 4.a and 4.b) show particles that consist of crystalline calcium aluminate with well-dispersed uniform Ni nanocrystals (black spots) in a wide distribution of sizes.

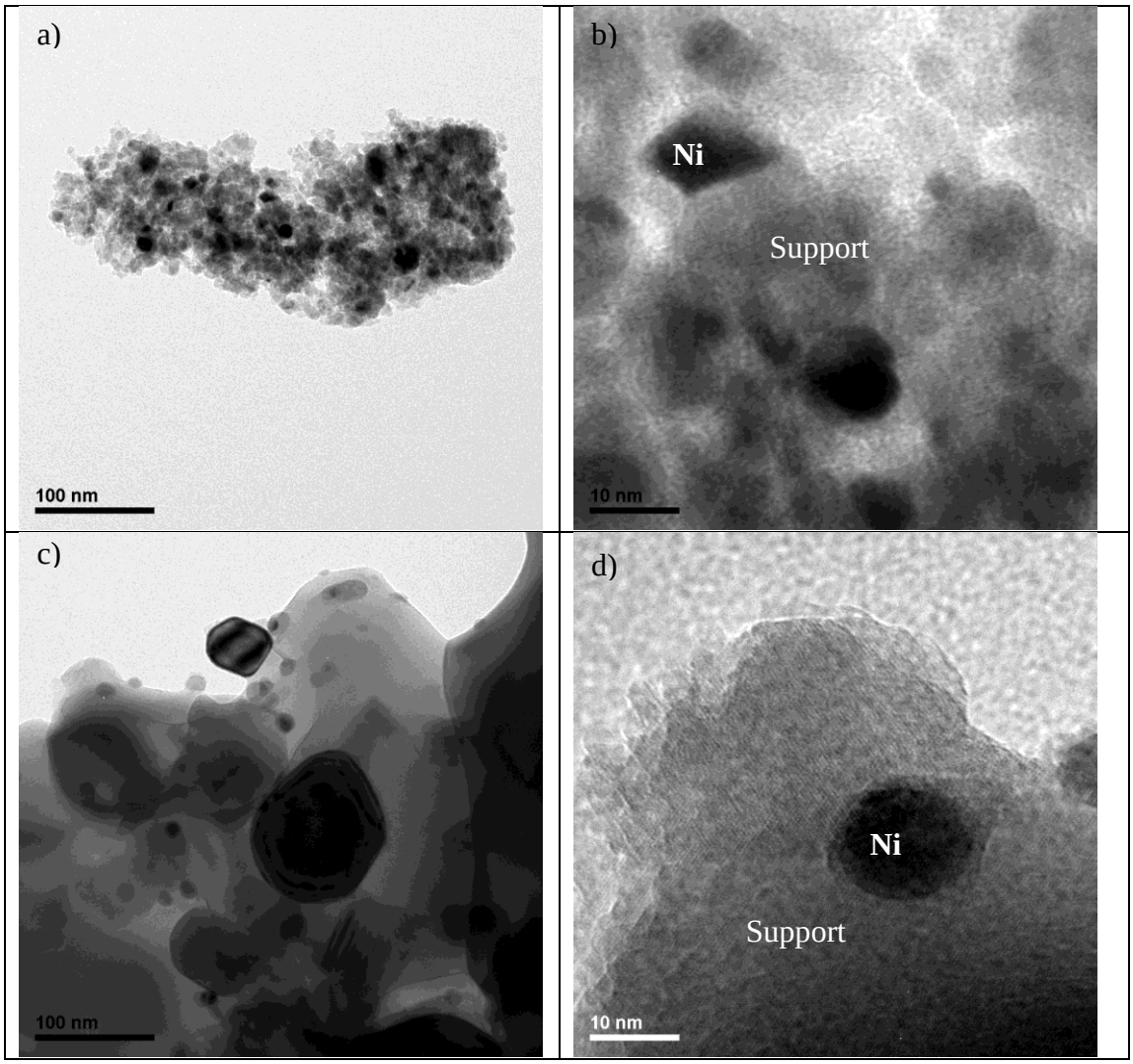

Fig. 4. Transmission electron microscopy images of Ni catalyst. a) reduced 1:100 nm, b) reduced 1:10 nm, c) 200 cycles and reduced 1:100 nm, d) 200 cycles and reduced 1:10 nm.

3.2. Steam-methane reforming tests

Several experiments were performed to identify the operational limits of the catalyst under study. For these tests the catalyst was mixed with an inert solid in order to closely monitoring the reforming activity and the evolution of catalyst properties. First, a wide range of temperatures was studied, ranging between 500 ºC and 700 ºC. The evolution of H_2, CH_4, CO and CO_2 concentrations (dry basis) in terms of the reforming temperature is plotted in Figure 5. Theoretical equilibrium concentrations calculated by means of HSC Chemistry software are also shown. It can be observed that

under the conditions of 2.0 $kgCH_4$ h^{-1} $kgcat^{-1}$ and 10 mlN min^{-1} CH_4, and a steam/methane ratio of 3, the experimental data are fairly close to the reaction equilibrium values of the four main components within the entire range of temperatures tested. Moreover, mass balances to carbon species are close to 95%, ensuring very low carbon deposition during this reaction.

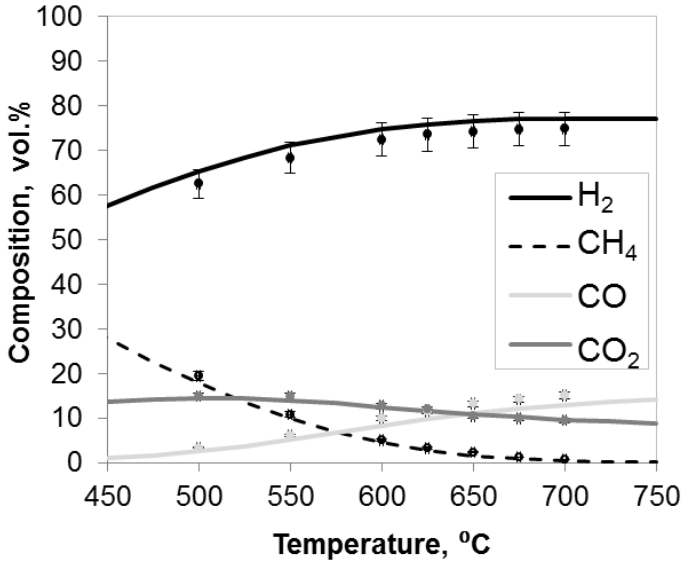

Fig. 5. Evolution of gas composition with reaction temperature. Space velocity 2.0 $kgCH_4$ h^{-1} $kgcat^{-1}$, 10 mlN min^{-1} CH_4, steam to methane molar ratio 3. Points are experimental values. Lines are theoretical values calculated by HSC 5.1

The effect of increasing MHSV and number of oxidation-reduction cycles on catalyst activity was also assessed (Figure 6). The MSHV was increased twice from 2.0 $kgCH_4$ h^{-1} $kgcat^{-1}$ to 4.3 $kgCH_4$ h^{-1} $kgcat^{-1}$, and to 8.8 $kgCH_4$ h^{-1} $kgcat^{-1}$, which is more than 10 times the optimal value calculated for a SE-SMR process coupled to a Ca/Cu cycle of 0.75 $kgCH_4$ h^{-1} $kgcat^{-1}$ [7]. In order to increase the MHSV the amount of catalyst and SiC used in the reaction bed was adjusted, at all times conforming to the plug flow criteria in the dispersion model reported by Levenspiel [47], and keeping the Péclet number higher than 800 [7]. At these demanding conditions, see Figure 6.a,

comparable experimental and theoretical equilibrium methane conversion results were obtained in the entire range of temperatures studied. Therefore, it can be concluded that the experiments were carried out with an excess of fresh catalyst that can be successfully used under these highly demanding operational conditions.

As previously explained, the SE-SMR process coupled to a Ca/Cu cycle alternates both reactants and conditions, sequentially leading to reforming, oxidation and calcination/reduction stages. The changes in the molar volumes associated with the oxidation of Ni to NiO and the further reduction to Ni could affect catalyst performance [10,36]. In order to determine the cyclic behaviour of the catalyst, the fresh catalyst sample was aged through 10 oxidation reduction cycles before studying the reforming reaction. Oxidation and reduction reactions were carried out in the fixed bed reactor system at 850 ºC under 10 vol.% O_2 (balanced by Ar) and 10 vol.% H_2 (balanced by Ar), respectively. CO_2 evolution was observed during the oxidation step owing to the deposition of coke on the catalyst surface throughout the reforming step (0.04 wt% kgcoke $kgcat^{-1}$). Figure 6.b shows the CH_4 conversion versus temperature for the SMR reaction for the fresh and aged catalyst performed at a steam to methane molar ratio of 3 and MHSV of 8.8 $kgCH_4$ h^{-1} $kgcat^{-1}$. Significantly, similar conversion values are found in both cases, which are very close to theoretical equilibrium values (continuous line in Figure 6) for the entire range of temperatures evaluated.

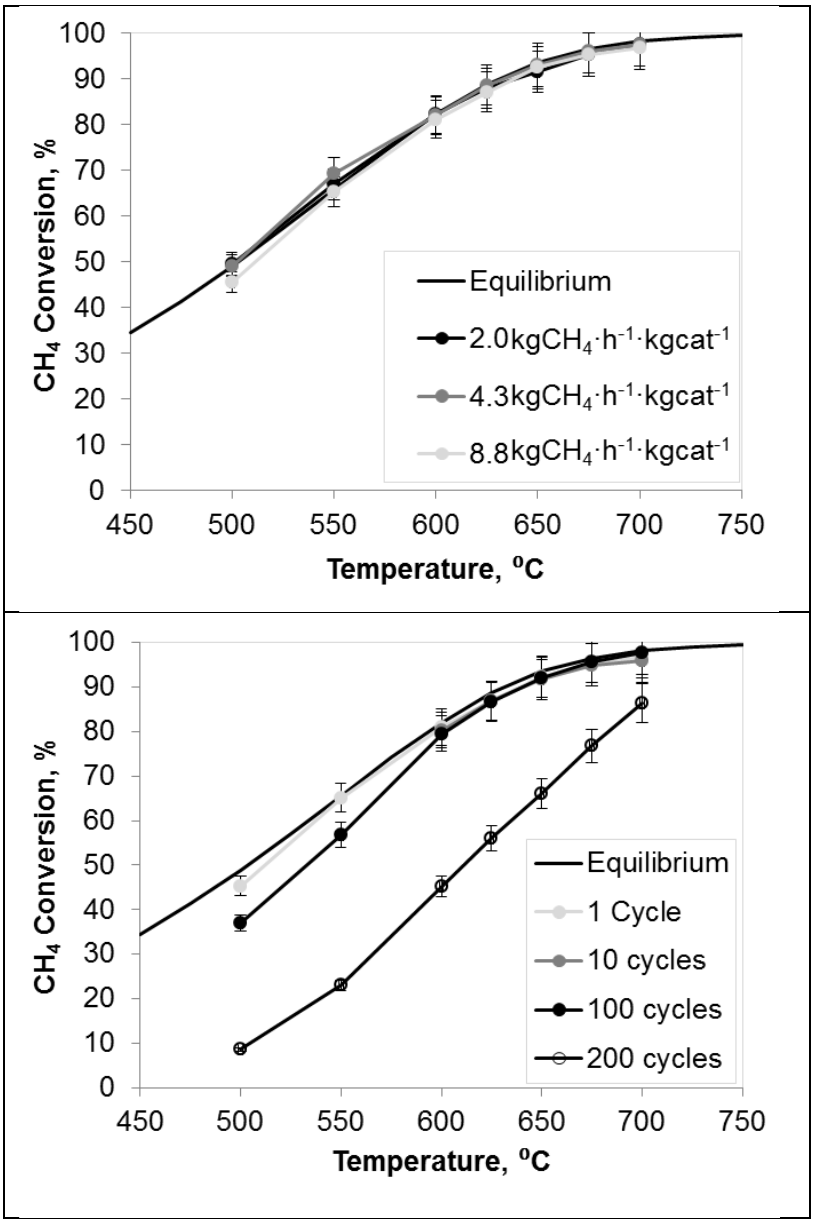

Fig. 6. Experimental CH_4 conversion and theoretical values obtained for Ni catalyst. 10 $mlN \cdot min^{-1} CH_4$, Steam to methane molar ratio 3. Points are experimental values. Lines are theoretical values calculated by HSC 5. a) Space velocity, b) Number of oxidation-reduction cycles (8.8 $kgCH_4\ h^{-1}\ kgcat^{-1}$).

Finally, a higher number of cycles were carried out to establish operational limits of the catalyst in a SE-SMR process coupled to Ca/Cu cycle. For this purpose, the catalyst was aged for 100 and 200 oxidation-reduction cycles (in a TGA system) before testing in the SMR reaction at a MHSV of 8.8 $kgCH_4\ h^{-1}\ kgcat^{-1}$ and temperatures ranging from 500 ºC to 700 ºC. The results obtained are also compiled in Figure 6.b and

compared to thermodynamic equilibrium data. After 100 oxidation-reduction cycles, although this catalyst maintains exceptional SMR activity under very demanding conditions its catalytic performance is slightly reduced from the equilibrium at temperatures lower than 600 ºC. The discrepancies between the experimental and theoretical data indicate that there are changes in the catalytic SMR kinetics; there is a possible reduction in reaction rates. With an increasing number of cycles, CH_4 conversion values for the sample cycled 200 times are comparable to calculated data in the temperature interval ranging between 600 ºC and 700 ºC (88% of the theoretical value calculated for equilibrium at 700 ºC) with more relevant differences between the experimental and equilibrium values at reforming temperatures below 600 ºC. Thus, CH_4 conversion at 500 ºC is only 17% of the theoretical value. The CO_2 evolution observed in the following oxidation step corresponded to a carbon deposition on the catalyst surface of 0.13 wt% kgcoke $kgcat^{-1}$. This value is slightly higher than the coke deposition calculated for the sample cycled 10 times. Nevertheless, both of them are small due to the high steam to carbon molar ratio of 3, which favours C gasification into CO. The structural and chemical properties of the cycled samples were determined in order to elucidate the causes of the decrease in catalytic activity with an increasing number of cycles.

The samples of the catalysts aged at 10, 100 and 200 oxidation-reduction cycles were mechanically separated from the inert material after the reforming test to perform XRD and SEM-EDX analyses. The results are compiled in Figure 2 and 3 with analysis of the initially reduced sample. It can be observed that the XRD patterns in Figure 2 for the aged samples are very similar to those of the fresh reduced catalyst, and show the existence of Al_2O_3, $Ca(Al_2O_3)_2$ and $CaO(Al_2O_3)$ phases, in addition to the metallic Ni phase. The strong interaction of Ca with Al_2O_3 to generate two calcium aluminates,

$CaO(Al_2O_3)_2$ and $CaOAl_2O_3$, prevents the formation of other phases in this material like $NiAl_2O_4$ spinel [48]. The formation of this very stable spinel phase may be a possible cause of deactivation, because it is not an active phase for methane reforming [43]. The crystallite size of Ni was calculated by the Rietveld method, and it was observed that this value increased from 9 nm (reduced sample) to 16 nm (10-cycle sample), 30 nm (100-cycle sample), and finally grew to 55 nm for the sample when cycled 200 times. The larger crystallite size of the Ni particles of the sample cycled 200 times is in line with the slightly higher carbon deposition observed for this sample compared to that attained for the sample after 10 cycles. An increase in Ni crystallite size has also been reported previously, regardless of the nature of the catalyst, the number of cycles, or the reforming-regeneration conditions [8,10,36,37]. Zhao et al. [8] and García-Lario et al. [10] with laboratory synthesised catalysts ($CaZrO_3$-stabilized 15 wt% Ni/CaO-$CaZrO_3$ bifunctional and 10 wt% NiO/$NiAl_2O_4$ catalysts) reported an increase in Ni crystallite size from 22.6 nm to 30.5 nm after 90 cycles, and from 117 nm to 121 nm in the first 19 cycles, respectively. Using commercial catalysts (12 wt% NiO/$CaAl_4O_7$), Lysicov et al. [36] observed an increase from 5 nm to 200 nm after 100 cycles, and Lopez-Ortiz and Harrison [37] also reported an increase in Ni crystallite size (18 wt% NiO/Al_2O_3) from 19.8 nm to 32.2 nm after 15 cycles.

SEM micrographs of the samples cycled 10, 100 and 200 times in reduced form are compared to those of the reduced fresh catalyst in Figure 3. Simultaneously, EDX analysis determined a similar Ni content in all the catalyst samples, which is seen to be concentrated in the brightest spots detected in the micrographs. The micrographs show the usual irregular surface of the support but with an increasing number and size of prevalent nano-sized Ni species, which are barely observed in the fresh catalyst. This observation suggests a modification in the superficial organization of Ni, likely due to

the either sintering of Ni crystallites with cyclic operation or the formation of surface aggregates [44]. Further examination by TEM of the catalyst cycled 200 times revealed considerable changes in the dispersion of the active component (Figures 4.c and 4.d). The initially reduced sample consists of nickel nanocrystals homogeneously distributed on the support. After 200 cycles, the particle size of some Ni particles increased to100–200 nm, as previously observed for nickel catalysts under redox cycling [36]. However, an apparently high number of Ni crystallites on the support were also found to still present a small size (around 10 nm). In short, although a sintering process of the Ni particles is obviously taking place, the residual presence of some nickel nanoparticles of small size after 200 oxidation-reduction cycles could explain the remaining activity observed under very demanding conditions.

To study the influence of the sintering process on catalyst reducibility, ten TPR/TPO cycles were performed. Figure 7 gives the data corresponding to the first TPR/TPO cycle of the fresh sample, as well as the profiles corresponding to the second, fifth and tenth cycles. In the first H_2-TPR run (Figure 7.a), three main peaks are observed with a total H_2 consumption of 67.2 cm^3 g^{-1}. The first peak at about 380 ºC is ascribed to the reduction of weakly bound NiO nanoparticles, commonly known as ‘free nickel’ [49]. Additionally, the second peak found at about 580 ºC could be attributed to either a bi-dimensional NiO monolayer [48] or small NiO nanoparticles with moderate interaction with the support. Finally, the third peak at the highest temperature of 700 ºC can be associated with the reduction of Ni species in notable interaction with the support, creating amorphous Ni-Ca-Al [48]. These species are predominant at the catalyst surface for the fresh sample.

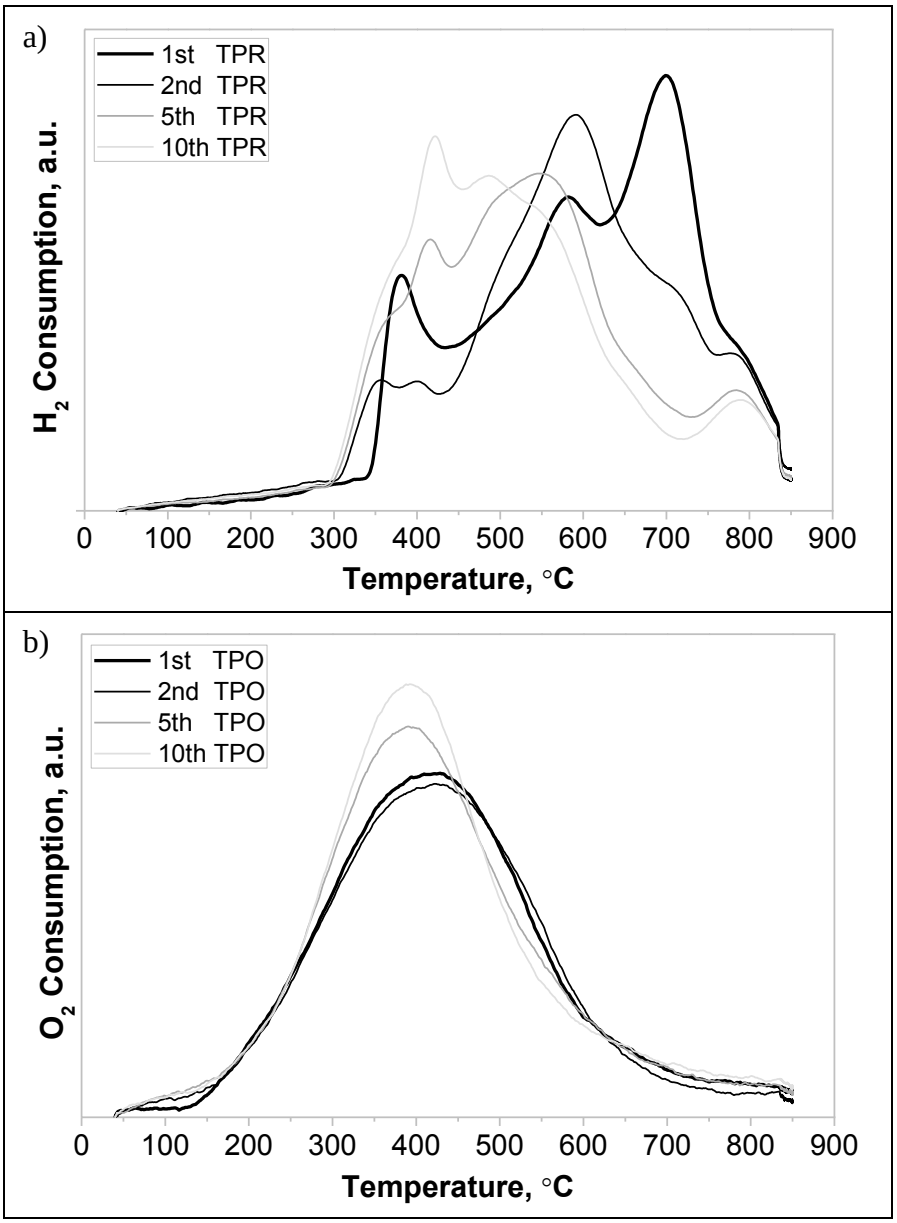

Fig. 7. (a) H_2-TPR and (b) O_2-TPO profiles of Ni catalyst.

The H_2 consumption calculated from the TPR, decreased from 67.2 cm^3 g^{-1} in the first cycle to a fairly constant value of 61.1 ± 1 cm^3 g^{-1}. Additionally, a redistribution of the Ni species is observed after consecutive oxidation-reduction cycles. Thus, Figure 7.a shows a shift in H_2 consumption towards lower temperatures between 300 ºC and 500 ºC [48]. This fact indicates that the prevalent amorphous Ni-Ca-Al species are transformed into NiO species with a weaker interaction with the support that improves material reducibility. This result is in line with a growth in the Ni crystallite

size during cyclic operation, as shown by XRD, SEM and TEM, leading to more reducible NiO species. The TPO obtained from the sample compiled in Figure 7.b, shows a similar form of O_2 consumption with increasing temperature for all the experiments with a maximum of about 400 ºC. Only a discrete increase in the amount of O_2 consumed by the different metallic Ni species is observed (26.1 cm^3 g^{-1} to 28.3 cm^3 g^{-1}). It can therefore be concluded that the increment in crystallite size, which agrees with an increase in reducible NiO species, may have a key role in the diminishing performance of the catalyst, and this is particularly evident under very demanding conditions (high space velocity and low temperature).

3.3. Sorption-enhanced steam-methane reforming tests

Once the operational limits of the catalyst under SMR conditions were achieved, the same catalyst was tested under the optimal conditions calculated for the reforming stage of an SE-SMR process coupled to a Ca/Cu cycle [7,15]. A sample of the catalyst cycled 200 times under oxidation-reduction conditions was mixed with a CaO-based sorbent with a sorbent to catalyst weight ratio of 4. This optimal value was selected taking into account both the Ni content of the catalyst and the CO_2 sorption capacity of the sorbent, as suggested in reference [15]. The sample bed was approximately 30 mm in length. The steam to methane molar ratio was increased to 4, the temperature was kept at 650 ºC, and more significantly, the MHSV was decreased to 0.75 $kgCH_4$ h^{-1} $kgcat^{-1}$ [7]. It is well known that space velocity is a significant operational parameter in the SE-SMR process since it affects both the hydrogen yield and CO_2 capture efficiency [15]. The key role of this parameter lies in the fact that carbonation is a significantly slower reaction than reforming [15]. Accordingly, low space velocities are required until more reactive CO_2 sorbents are developed. Optimal pressure for this stage is described in the range between 5 bar and 15 bar because it favours H_2 production to

feed gas turbines for power generation, and it favours Cu oxidation, which is the following stage in this SE-SMR process coupled to a Ca/Cu cycle. However, the tests were conducted at atmospheric pressure to focus on the effect that the oxidation-reduction cycles might have on catalyst performance. Any evidence of diminishing catalytic activity under these conditions would also be found to occur at higher pressures. Under these conditions, the Cu-based materials suitable for this process will act as inert material because Cu presents low WGS activity [50] and the final gas product composition will mainly be determined by sorbent reactivity [7,15]. Copper could also promote methane decomposition to accelerate carbon deposition. However, the high steam to carbon molar ratio would favour carbon gasification into CO. The introduction of the Cu solid into the reactor would affect the thermal ballast and would reduce the available isothermal volume of the system to allocate the sorbent. This last factor will shorten the duration of the H_2 production stage, which will end when the sorbent becomes saturated. For these reasons, in order to ensure an effective test focused on proving the application of the highly cycled commercial Ni catalyst, the copper solid was not included. For comparative purposes, the catalyst cycled 200 times was also tested for SMR process under these new experimental conditions, see Figures 8.a and 8.b. These results show that the system is able to reach a theoretical equilibrium composition between 650 ºC and 700 ºC. However, only 87% of the maximum CH_4 conversion calculated from thermodynamics is achieved (Figure 8b) at 600 ºC.

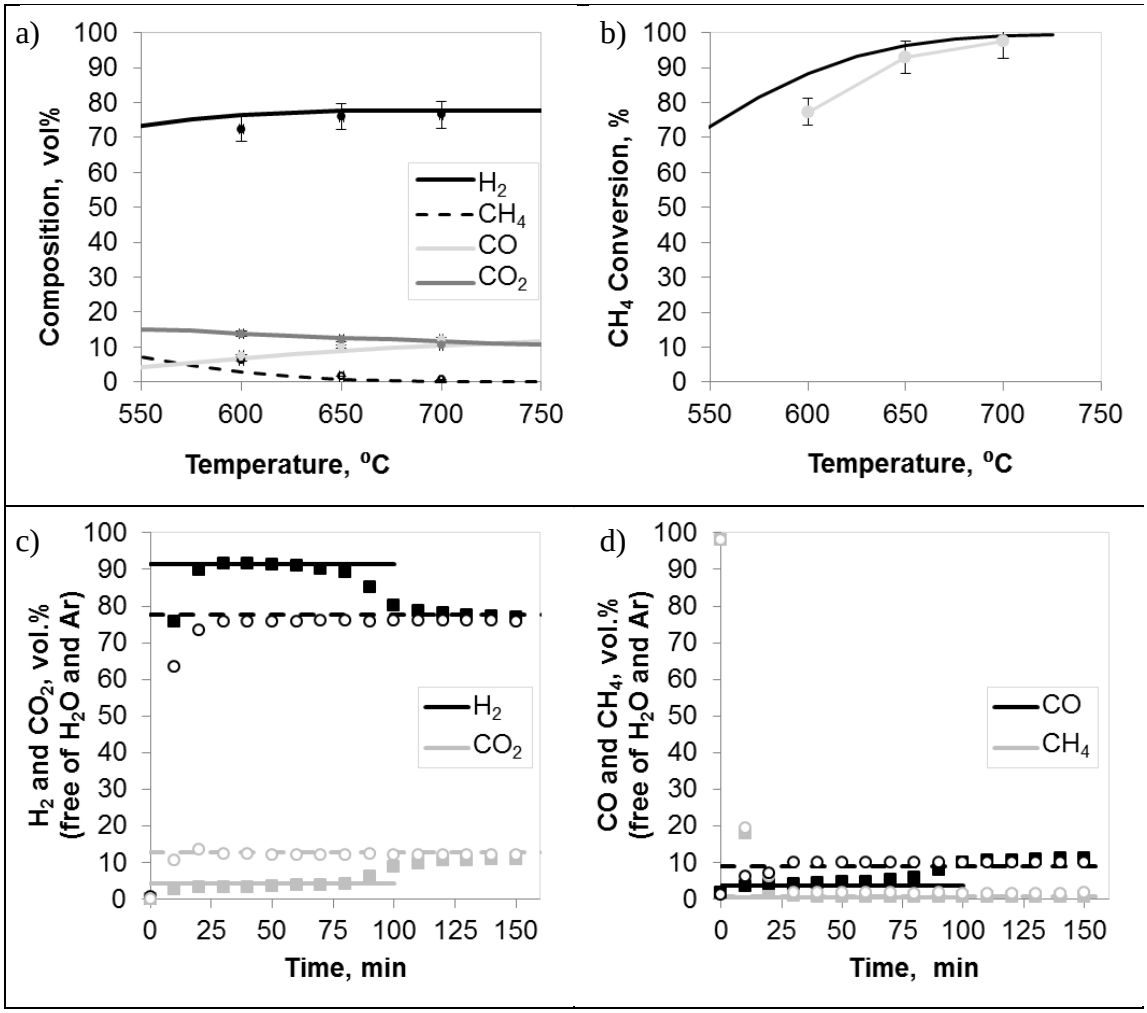

Fig. 8. Experimental results for Ni catalyst cycled 200 times in oxidation-reduction stages. Space velocity 0.75 $kgCH_4$ h^{-1} $kgcat^{-1}$, 1.7 mlN min^{-1} CH_4, steam to methane molar ratio 4. SMR test (a) Evolution of gas composition (b) and CH_4 conversion with temperature. SE-SMR test at 650 ºC with a mixture sorbent to catalyst ratio of 4 (squares) and without sorbent (circles). (c) H_2 and CO_2 concentration evolution and (d) CO and CH_4 evolution with time. Points are experimental values. Lines (SE-SMR solid, SMR dashed) are theoretical values calculated by HSC 5.1.

On the other hand, Figures 8c and 8d show the experimental results obtained in the micro fixed-bed reactor with the catalyst/sorbent mixture in terms of evolution of the product gas composition with time. For the sake of comparison, the performance of the catalyst at the same process conditions without sorbent is also plotted in Figures 8c and 8.d. When there is not sorbent present in the reaction bed, the cycled catalyst is notably active towards SMR and the product composition reaches stable values (circles) close to the theoretical equilibrium data (dashed lines). Upon 150 minutes time-on-

stream, the catalyst presents no evidences of deactivation. As seen, the experimental curves obtained with the mixture catalyst/sorbent present the three typical stages widely described in the literature for SE-SMR experiments [5]: i) pre-breakthrough, when the reforming, water gas shift and carbonation reactions take place at the same time; ii) breakthrough, when the sorbent starts to become saturated and CO_2 removal starts to decrease until the sorbent is totally saturated and; iii) post-breakthrough, when the sorbent is saturated so that CO_2 sorption is no longer effective and only reforming and water gas shift reactions take place. Figure 8 shows that the H_2 concentration reaches 92 vol.% after a time delay caused by the system dead volume. This value is in close agreement with equilibrium calculations. The stable composition in this period is typical of a pre-breakthrough step when CaO is reacting with CO_2, which allows high methane to hydrogen conversion to produce high-purity hydrogen. The beginning of the breakthrough corresponds to the carbonation front of reaction reaching the end of the solid bed. CO_2 removal efficiency decreases, thereby reducing the key role of the sorbent-shifting SMR and WGS reactions. From this point, CO_2 concentration clearly increases as well as CO, while H_2 concentration decreases. The second steady-state period of this experiment produces a H_2 concentration of 77 vol.%, which is also very close to the theoretical equilibrium data obtained in the test without sorbent, when only SMR and WGS reactions take place. With regard to CH_4 conversion under these experimental conditions, the change from pre-breakthrough to post-breakthrough is not important, in line with thermodynamic equilibrium data, with a CH_4 conversion higher than 96% in both stages. By comparing results from Figure 8, it can be appreciated that the activity showed by the catalyst at 650 ºC was high enough for the SE-SMR stage at the optimal conditions selected for the process coupled to a Ca/Cu cycle. These positive results produced after a high number of oxidation-reduction cycles, support the use of

this commercial Ni-based catalyst in the next development steps of the process in the range of optimal MHSV and steam to methane molar ratio, and in the temperature calculated for the process [15]. However, further experimental and theoretical research is needed to model the changes observed after cycling in the catalytic steam-reforming kinetics under more demanding conditions. Based on it, future work on reforming catalysts could be focused on improving the long-term reactivity in the cyclic application. Furthermore, it is well known that different sorbent-related factors such as CO_2 removal and sorbent to catalyst ratio can affect the performance of these systems [27], and therefore the influence of these parameters need to be carefully evaluated in an increasing number of cycles.

4. Conclusions

Evaluation was made of the operational limits of a commercial Ni-based catalyst provided by Johnson Matthey© (HiFUEL® R110) under the typical conditions of sorption-enhanced steam-methane reforming coupled to a Ca/Cu process. The steam reforming activity of this material was studied under different conditions of temperature and MHSV, and its stability was measured after multi-cycle oxidation-reduction tests. After 100 oxidation-reduction cycles at 850 ºC, this catalyst showed remarkable activity for a wide range of temperatures between 500 ºC and 700 ºC, and MHSV between 2.0 $kgCH_4\ h^{-1}\ kgcat^{-1}$ and 8.8 $kgCH_4\ h^{-1}\ kgcat^{-1}$. However, after the sample was cycled 200 times, it already showed a significant reduction in its reforming activity under the most demanding conditions, and was unsuccessful in achieving the theoretical equilibrium values. The characterization of the catalyst by different complementary techniques after oxidation-reduction cycles showed a progressive increase in the mean Ni crystallite size from 10 nm to 55 nm, although the presence of some small Ni nanocrystallites was still

evident. This may be linked to the partial deactivation of the catalyst. Once the operational limits of the catalyst were established, a mixture of the aged catalyst cycled 200 times with a CaO-based sorbent was tested under the optimal conditions for SE-SMR coupled to a Ca/Cu looping process. Significantly, theoretical thermodynamic equilibrium data were completely met and a H_2 concentration of more than 92 vol.% was reached. These positive results demonstrate that this catalyst is a very promising candidate to be used in the next steps of the scale-up process.

Acknowledgments

The authors acknowledge support received from the European Union Seventh Framework Programme FP7 under grant agreement No. 608512 (ASCENT Project) and the Regional Government of Aragon (DGA) under the research groups support programme. The authors wish to thank J.M. Pardo for participating in the experimental work.

REFERENCES

[1] Report of the Hydrogen Production Expert panel: A subcommittee for the Hydrogen & fuel Cell Technical Advisory Committee. United States Department of Energy, Washington, DC, May 2013.

[2] M.V. Gil, J. Fermoso, C. Pevida, D. Chen, F. Rubiera, Production of fuel-cell grade H_2 by sorption enhanced steam reforming of acetic acid as a model compound of biomass-derived bio-oil, Appl. Catal. B: Environ. 184 (2016) 64-76.

[3] R. Soltani, M.A. Rosen, I. Dincer, Assessment of CO_2 capture options from various points in steam methane reforming for hydrogen production, Int. J. Hydrogen 39 (2014) 20266-20275.

[4] B. Chen, Z. Liao, J. Wang, H. Yu, Y. Yang, Exergy analysis and CO_2 emission evaluation for steam methane reforming, Int. J. Hydrogen Energy 37 (2012) 3191-3200.

[5] D.P. Harrison, Sorption-Enhanced Hydrogen Production: a review, Ind. Eng. Chem. Res. 47 (2008) 6486-6501.

[6] M. S. Yancheshmeh, H.R. Radfarnia, M.C. Iliuta, High temperature CO_2 sorbents and their application for hydrogen production by sorption enhanced steam reforming process, Chem. Eng. J. 283 (2016) 420-444.

[7] J.R. Fernandez, J.C. Abanades, R. Murillo, Modeling of sorption enhanced steam methane reforming in an adiabatic fixed bed reactor, Chem. Eng. Sci. 84 (2012) 1-11.

[8] C. Zhao, Z. Zhou, Z. Cheng, X. Fang, Sol-gel-derived, $CaZrO_3$-stabilized Ni/CaO-$CaZrO_3$ bifunctional catalyst for sorption-enhanced steam methane reforming, Appl. Catal. B: Environ. 196 (2016) 16-26.

[9] S.A. Bhat, J. Sadhukhan, Process intensification aspects for steam methane reforming: and overview, AIChE J. 55 (2009) 408-422.

[10] A.L. García-Lario, M. Aznar, G.S. Grasa, R. Murillo, Evaluation of process variables on the performance of Sorption Enhanced Methane Reforming, J. Power Sources 285 (2015) 90-99.

[11] J.C. Abanades, R. Murillo, J.R. Fernandez, G. Grasa, I. Martínez, New CO_2 capture process for hydrogen production combining Ca and Cu chemical loops, Environ. Sci. Technol 44 (2010) 6901-6904.

[12] J.C. Abanades, R. Murillo, 2009, PCT/ES2010/0705852009.

[13] J.R. Fernandez, J.C. Abanades, Overview of the Ca-Cu looping process for hydrogen production and/or power generation, Curr. Op. Chem. Eng. 17 (2017) 1-8.

[14] J.R. Fernandez, J.C. Abanades, R. Murillo, G. Grasa, Conceptual design of a hydrogen production process from natural gas with CO_2 capture using a Ca-Cu chemical loop, Int. J. Greenh. Gas Control 6 (2012) 126-141.

[15] J.R. Fernandez, J.C. Abanades, G. Grasa, Modeling of sorption enhanced steam methane reforming-Part II: Simulation within a novel Ca/Cu chemical loop process for hydrogen production, Chem. Eng. Sci. 84 (2012) 12-20.

[16] J.R. Fernández, J.C. Abanades, R. Murillo, Modeling of Cu oxidation in adiabatic fixed-bed reactor with N2 recycling in a Ca/Cu chemical loop, Chem. Eng. J. 232 (2013) 442–452.

[17] M. Martini, A. van den Berg, F. Galluci, M. Sint Annaland, Investigation of the process operability windows for Ca-Cu looping for hydrogen production with CO_2 capture, Chem. Eng. J. 303 (2016) 73-88.

[18] I. Martinez, R. Murillo, G. Grasa, J.R. Férnandez, J.C. Abanades, Design of a hydrogen production process for power generation based on a Ca-Cu chemical loop, Energy Procedia 37 (2013) 626–634.

[19] I. Martinez, R. Murillo, G. Grasa, J.R. Fernandez, J.C. Abanades, Integrated combined cycle from natural gas with CO_2 capture using a Ca-Cu chemical loop, AIChE J. 59 (2013) 2780–2794.

[20] I. Martínez, M.C. Romano, J.R. Fernández, P. Chiesa, R. Murillo, J.C. Abanades, Process design of a hydrogen production plant from natural gas with CO_2 capture based on a novel Ca/Cu chemical loop, Appl. Energy 114 (2014) 192–208.

[21] J.R. Fernandez, J.C. Abanades, Optimized design and operation strategy of Ca-Cu chemical loop process for hydrogen production, Chem. Eng. Sci. 166 (2017) 144-160.

[22] A.L. García-Lario, I. Martínez, R. Murillo, G. Grasa, J.R. Fernández, J.C. Abanades, Reduction kinetics of a high load Cu-based pellet suitable for Ca/Cu chemical loops. Ind. Eng. Che. Res. 52 (2013) 1481-1490.

[23] C. Qin, B. Feng, J. Yin, J. Ran, L. Zhang, V. Manovic, Matching of kinetics of $CaCO_3$ decomposition and CuO reduction with CH_4 in Ca-Cu chemical looping, Chem. Eng. Sci, 262 (2015) 665-675.

[24] J.M. Alarcon, J.R. Fernandez, Study of Cu-CuO chemical loop for the calcination of $CaCO_3$ in a fixed bed reactor. Chem. Eng. J. 325 (2017) 208-220.

[25] G. Grasa, M.V. Navarro, J.M. López, L. Díez-Martín, J.R. Fernández, R. Murillo, Validation of the H_2 production stage via SER under relevant conditions for the Ca/Cu reforming process practical application, Chem. Eng. J. 324 (2017) 266-278.

[26] J.R. Hufton, S. Mayorga, S. Sircar, Sorption-Enhanced Reaction Process for Hydrogen production, AIChE J. 45 (1999) 248-256.

[27] K. Johnsen, H.J. Ryu, J.R. Grace, C.J. Lim, Sorption-enhanced steam reforming of methane on a fluidized bed reactor with dolomite as CO_2-acceptor, Chem. Eng. Sci. 61 (2006) 1195-1202.

[28] D.K. Lee, I.H. back, W.L. Yoon, Modeling and simulation for the methane steam reforming enhanced by in situ CO_2 removal utilizing the CaO carbonation for H_2 production, Chem. Eng. Sci. 59 (2004) 931-942.

[29] K.B. Yi, D.P. Harrison, Low-pressure sorption-enhanced hydrogen production, Ind. Eng. Chem. Res. 44 (2005) 1665-1669.

[30] K. Essaki, T. Muramatsu, M. Kato, Effect of equilibrium shift by using lithium silicate pellets in methane steam reforming, Int. J. Hydrogen Energy 33 (2008) 4555-4559.

[31] B. Balasubramanian, A. Lopez-Ortiz, S. Kaytakoglu, D.P. Harrison, Hydrogen from methane in a single-step process, Chem. Eng. Sci. 54 (1999) 3543-3552.

[32] M.G. Beaver, H.S. Caram, S. Sircar, Sorption enhanced reaction process for direct production of fuel-cell grade hydrogen by low temperature catalytic steam-methane reforming, J. Power Sources 195 (2010) 1998-2002.

[33] Y. Ding, E. Alpay, Adsorption-enhanced steam-methane reforming, Chem. Eng. Sci. 55 (2000) 3929-3940.

[34] C.H. Lee, S. Mun, K.B. Lee, Application of multisection packing concept to sorption-enhanced steam methane reforming reaction for high-purity hydrogen production, J. Power Sources 281 (2015) 158-163.

[35] E.L.G. Oliveira, C.A. Grande, A.E. Rodrigues, Steam methane reforming in a Ni/Al_2O_3 catalyst: kinetics and diffusional limitations in extrudates, Can. J. Chem. Eng. 87 (2009) 945-956.

[36] A. Lysikov, A. Okunev, O. Netskina, Study of a nickel catalyst under conditions of the SER process: Influence of RedOx cycling, Int. J. Hydrogen Energy 38 (2013) 10354-10363.

[37] A. Lopez-Ortiz, D. P. Harrison, Hydrogen production using sorption-enhanced reaction, Ind. Eng. Chem. Res. 40 (2001) 5102-5109.

[38] Z.S. Li, N.S. Cai, J.B. Yang, Continuous production of hydrogen from sorption-enhanced steam methane reforming in two parallel fixed-bed reactors operated in cyclic manner Ind. Eng. Chem. Res.,45 (2006) 8788-8793.

[39] C.S. Martavaltzi, E.P. Pampaka, E.S. Korkakaki, A.A. Lemonidou, Hydrogen production via steam reforming of methane with simultaneous CO_2 capture over CaO-$Ca_{12}Al_{14}O_{33}$, Energy Fuels 24 (2010) 2589-2595.

[40] K.D. Dewoolkar, P.D. Vaidya, Improved hydrogen production by sorption-enhanced steam methane reforming over hydrotalcite- and calcium-based hybrid materials, Energy Fuels 29 (2015) 3870-3878.

[41] B. Dou, C. Wang, Y. Song, H. Chen, B. Jiang, M. Yang, Y. Xu, Solid sorbents for in-situ CO_2 removal during sorption-enhanced steam reforming process: a review, Renew. Sustain. Energy Rev. 53 (2016) 536-546.

[42] S.D. Angeli, G. Monteleone, A. Giaconia, A.A. Lemonidou, State-of-the-art catalysts for CH_4 steam reforming at low temperatures, Int. J. Hydrogen Energy 39 (2014) 1979-1997.

[43] A.L. García-Lario, M. Aznar, G.S. Grasa, T. García, R. Murillo, Study of nickel catalysts for hydrogen production in sorption enhanced reforming process, J. Power Sources 242 (2013) 371-379.

[44] J.A. Medrano, H.P. Hamers, G. Williams, M. van Sint Annaland, F. Galluci, NiO/$CaAl_2O_4$ as active oxygen carrier for low temperature chemical looping applications, Appl. Energy 158 (2015) 86-96.

[45] A.L. García-Lario, M. Aznar, I. Martinez, G.S. Grasa, T. García, R. Murillo, Experimental study of the application of a NiO/$NiAl_2O_4$ catalyst and a CaO-based synthetic sorbent on the Sorption Enhance Reforming process, Int. J. Hydrogen Energy 40 (2015) 219-232.

[46] V. Manovic, E.J. Anthony, Long-term behaviour of CaO-based pellets supported by calcium aluminate cements in a long series of CO_2 capture cycles, Ind. Eng. Chem. Res. 48 (2009) 8906-8912.

[47] O.S. Levenspiel, The chemical reactor Omnibook, Oregon State University Book Stores, 1979, chapter 64.

[48] C.K.S. Choong, Z. Zhong, L. Huang, Z. Wang, T. Peng Ang, A. Borgna, J. Lin, L. Hong, L. Chen, Effect of calcium addition on catalytic ethanol steam reforming of Ni/Al_2O_3: I. Catalytic stability, electronic properties and cocking mechanism, Appl. Catal. A: Gen. 407 (2011) 145-154.

[49] A. Cabello, P. Gayán, F. García-Labiano, L.F. de Diego, A. Abad, M.T. Izquierdo, J. Adanez, Relevance of the catalytic activity on the performance of a NiO/$CaAl_2O_4$ oxygen carrier in a CLC process, Appl. Catal. B: Environ. 147 (2015) 980-987.

[50] L. Gradisher, B. Dutcher, M. Fan, Catalytic hydrogen production from fossil fuels via the water gas shift reaction, Appl. Energy, 139 (2015) 335-349.